

Multiphase density functional theory parameterization of the Gupta potential for silver and gold

John T. Titantah¹ and Mikko Karttunen²

¹*Department of Applied Mathematics, The University of Western Ontario,
1151 Richmond St. N., London, Ontario, Canada, N6A 5B7**

²*Department of Chemistry, University of Waterloo, 200 University Avenue West, Waterloo, Ontario, Canada, N2L 3G1[†]*
(Dated: November 19, 2012)

The ground state energies of Ag and Au in the face-centered cubic (FCC), body-centered cubic (BCC), simple cubic (SC) and the hypothetical diamond-like phase, and dimer were calculated as a function of bond length using density functional theory (DFT). These energies were then used to parameterize the many-body Gupta potential for Ag and Au. This parameterization over several phases of Ag and Au was performed to guarantee transferability of the potentials and to make them appropriate for studies of related nanostructures. Depending on the structure, the energetics of the surface atoms play a crucial role in determining the details of the nanostructure. The accuracy of the parameters was tested by performing a 2 ns MD simulation of a cluster of 55 Ag atoms – a well studied cluster of Ag, the most stable structure being the icosahedral one. Within this time scale, the initial FCC lattice was found to transform to the icosahedral structure at room temperature. The new set of parameters for Ag was then used in a temperature dependent atom-by-atom deposition of Ag nanoclusters of up to 1000 atoms. We find a deposition temperature of 500 ± 50 K where low energy clusters are generated, suggesting an optimal annealing temperature of 500 K for Ag cluster synthesis.

PACS numbers: 61.46.Df, 36.40.-c, 71.15.Mb, 12.39.Pn

I. INTRODUCTION

Applications of noble metal nanoparticles are currently emerging in medicine where they are used as antimicrobial agents¹, antivirals against HIV-1², antiangiogenic agents³, in drug delivery⁴ and in cancer therapy^{4,5}. They are also used in chemical sensory devices due to their enhanced surface chemical activity⁶⁻¹⁰. Ag clusters as small as Ag₇ and Ag₈ supported with mercaptosuccinic acid have been demonstrated to be very potent in water purification through their chemical sensitivity to the presence of heavy metals like Pb, Cd, Hg¹¹. The application of noble metal nanoparticles in the electronic industry in inkjet printing of conductive lines for circuitry¹² and as electronically conductive adhesives¹³⁻¹⁶ results from their electronic properties. Organic memory devices based on DNA biopolymer nanocomposites with Ag nanoparticles have been demonstrated¹⁷. The large optical forces induced by the transfer of momentum from electromagnetic radiation to a dielectric nanoparticle also make them useful in nano optical manipulation^{7,18-20}. It has been shown that subjecting Au nanoparticles to optical forces induces aggregation and enhances the Raman scattering intensity of the thiophenol coverage of the Au nanoparticle²¹.

It is common to synthesize noble metal nanoparticle either as free standing or in an inert gas matrix with sizes ranging from one to several hundred of nanometers. Ag nanoclusters as small as 4.1 nm and 5.6 nm have been deposited on silicon substrates. Their thermally induced disintegration has been studied, revealing melting at temperatures well below Ag melting temperature²². Clusters of few atoms are also routinely isolated by stabilizing them with some protective molecules^{22,23}. For example, a 25 atom Au-thiolate cluster in solution²⁴, dodecanethiol-stabilized-Au₃₈²⁵, a 1 nm lysozyme-stabilized-Au nanocluster for Hg²⁺ sensor²⁶ and DNA-encapsulated 10 atom Ag-cluster²⁷ have been reported. A small angle X-ray study on the mechanism of Ag nanopar-

ticle formation showed that nanoparticle formation initiates with the formation of Ag₁₃ clusters which agglomerate together to form a nanoparticle within 6 ms²⁸.

The advances in synthesis methods have not been accompanied by an equal increase in understanding of the structural, electronic and optical properties. The nanosized nature gives these particles/clusters properties that are intermediate between molecular, which are of quantum origin, and bulk character. Size dependent structural changes have been widely investigated using methods ranging from experiments based on electron diffraction spectroscopy^{29,30} to theoretical methods involving classical molecular mechanics approaches³¹ and quantum calculations. In particular, pseudopotential time-dependent density functional theory (TDDFT) calculations of the optical absorption of magic number noble metal nanoparticles have been carried out³². Crossover from molecular to nanosized behavior was predicted to occur for clusters with more than 150 Ag atoms³². Calculations of the absorption and the Raman enhancement of Ag_n-pyridine complexes (n=2-20) have been done using TDDFT and both properties were found to depend strongly on the cluster size³³.

Theoretical studies of noble metal clusters are widely based on classical approaches making use of interatomic potentials like the Gupta potential^{34,35}, the Sutton-Chen potential^{36,37} and the embedded atom potential^{38,39}. The latter has been used to study the size dependent melting of Ag nanocluster⁴⁰, spontaneous alloying in Au-Ag nanoclusters³⁹ and structural optimization of Ag-Pd⁴¹. The Gupta potential is widely used in predicting stable structures of noble metal nanoparticles like Ag and Au⁴² and bimetallic clusters like Pd-Au⁴². The parameters of the potential are obtained by fitting experimental or DFT⁴² data on the bulk face-centered cubic (FCC) system. This does not, however, guarantee transferability of the potential to the different phases of the system. For example, when the resulting potentials are applied to lower coordination states of the material (such as dimers, trimers, etc.), very short

bonds and overbinding are obtained rendering the potential inappropriate for studies of low dimensional objects like nanoclusters. This effect has also been demonstrated to explain the finding that the Gupta and Sutton-Chen parameterizations predict different growth patterns already for small Ag clusters⁴³. Shao *et al.*⁴³ pointed out that due to the flatter nature of the dimer potential as given by the Gupta formulation, it is susceptible to yield more strain-tolerant structures than those generated using the Sutton-Chen potential.

In this study, we use the DFT approach to perform ground state energy calculations on the FCC, BCC, simple cubic, the hypothetical diamond-like phase and dimer. These energy profiles are used to parameterize the Gupta potential. The parameters are given as functions of the coordination number of the Ag and Au atoms-giving them a bond-order character. The appropriateness of the parameters for low coordinated structures is demonstrated.

II. ALL ELECTRON CALCULATION: PARAMETERIZATION OF THE GUPTA POTENTIAL

We used the WIEN2k all-electron-full-potential linearized-augmented-plane-wave DFT code⁴⁴ to calculate the binding energies of Ag and Au in FCC, BCC, simple cubic, diamond-like phases, and dimers. This DFT approach partitions the unit cell into muffin-tin (MT) spheres centered on each atomic site and the interstitial region. Within the MT spheres, the Kohn-Sham functions are given as linear combinations of spherical harmonics weighted by radial functions. In the interstitials they are parameterized as plane-waves. The generalized gradient approximation (GGA)⁴⁵ for the exchange and correlation energy is adopted. The two parameters governing the accuracy of the calculation are the number of plane-waves in the Brillouin zone and the plane-wave vector \mathbf{k} cut-off parameter - RKM . This latter parameter is the product of the maximum plane wave vector in the interstitial region and the smallest muffin-tin radius in the system. For our calculations, the total number of k -points ranged from 1000 to 3000, depending on the system and RKM value of 6 were found to converge the binding energies to an accuracy of 3 mRy per atom.

Non-magnetic calculations were performed since both bulk Ag and Au are known to be non-magnetic. For each of the noble metal structures, energy-bond length dependencies were obtained. From them, extrapolation to very large lattice parameters permitted the isolated atom values to be removed yielding the binding energies as shown in Figs 1 and 2. For FCC Ag, we find an equilibrium lattice parameter of 4.07 ± 0.02 Å and a binding energy of 3.16 ± 0.04 eV/atom. The former compares very well with the measured value of 4.09 Å while the binding energy overestimates the measured value of 2.95 eV⁴⁶ by about 7 %. The bulk modulus was found to be 106 ± 2 GPa which is in excellent agreement with the experimental value of 109 GPa at 0 K⁴⁷. For Au, a lattice parameter of 4.09 ± 0.02 Å (see Fig. 3(a)) compares very well with the measured value of 4.08 Å. The binding energy of 4.01 ± 0.04 eV, however, overestimates the experimental value of 3.81 eV^{46,48,49}. The bulk modulus of 179 ± 2 GPa is in ex-

cellent agreement with experimentally measured value of 180 GPa at 0 K⁴⁷.

The BCC phase is less stable than the FCC phase by about 0.06 (0.08) eV/atom for Ag (Au) and is thus predicted to be the high pressure phase of these materials. This is in agreement with another theoretical work that predicted the same result for Au⁵⁰. The small energy difference between the BCC and the FCC phases of Ag is a possible reason for the recently observed continuous and reversible BCC-FCC phase transformation in Ag/V multilayers⁵¹.

We used these energy-lattice parameter (or energy-bond length E - r) dependencies to parameterize the Gupta potential for Ag and Au. For this, we rescaled the binding energies by a factor of 0.934 (0.951) for Ag (Au) to equate the FCC value with the measured value while rescaling distances by a factor of 1.006 (0.996) for Ag (Au) to equate to the corresponding FCC experimental bond length of 2.889 Å (2.884 Å). With these, the bulk moduli become 99 GPa for Ag and 170 GPa for Au. Most of the parameterizations that have been done are based on the bulk properties in the FCC phase^{42,43}. To our knowledge, this is the first attempt to develop parameters that make the potential transferable enough for use in various phases. These new parameters should therefore be appropriate in high temperature studies of these metals and for low-dimensional structures formed from them.

For this potential, the energy of atom i is given by⁵²

$$V_i = V_i^r - V_i^a, \quad (1)$$

where the repulsive part of the potential is given by

$$V_i^r = \frac{1}{2} \sum_{j \neq i} \alpha \exp \left[-\lambda \left(\frac{r_{ij}}{R_0} - 1 \right) \right] \quad (2)$$

and the attractive part by

$$V_i^a = \frac{1}{2} \left[\sum_{j \neq i} \beta^2 \exp \left[-2\mu \left(\frac{r_{ij}}{R_0} - 1 \right) \right] \right]^{1/2}. \quad (3)$$

In the first approximation, the phase dependence of this potential is introduced by adopting a coordination dependence of the parameters; where coordination is defined by introducing a cut-off function f_c

$$f_c(x) = \begin{cases} 1 & \text{for } x \leq 3.1 \text{ Å} \\ 0 & \text{for } x > 3.1 \text{ Å} \end{cases} \quad (4)$$

by which coordination n_{ci} is given by

$$n_{ci} = \sum_{j \in \text{Nei}(i)} f_c(r_{ij}), \quad (5)$$

where $\text{Nei}(i)$ is the set of nearest neighbor atoms of atom i . The choice of a cut-off distance of 3.1 Å was made to exclude the next nearest neighbor atoms of the BCC phase that show up beyond 3.2 Å for both Ag and Au.

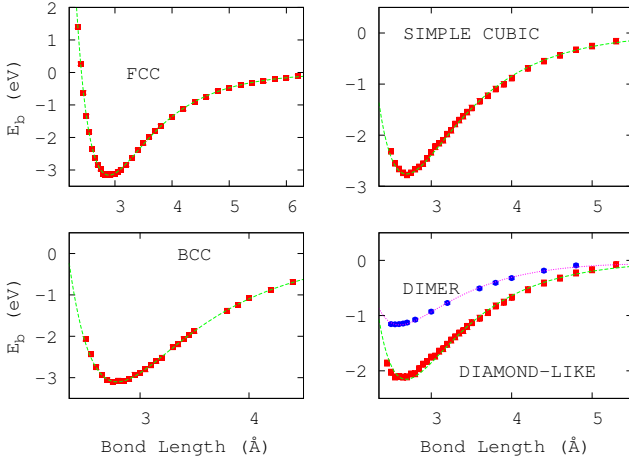


FIG. 1. Energy per Ag atom as a function of distance between atoms for five phases of Ag: face-centered cubic, body-centered cubic, simple cubic, Ag in the diamond-like phase and Ag dimer.

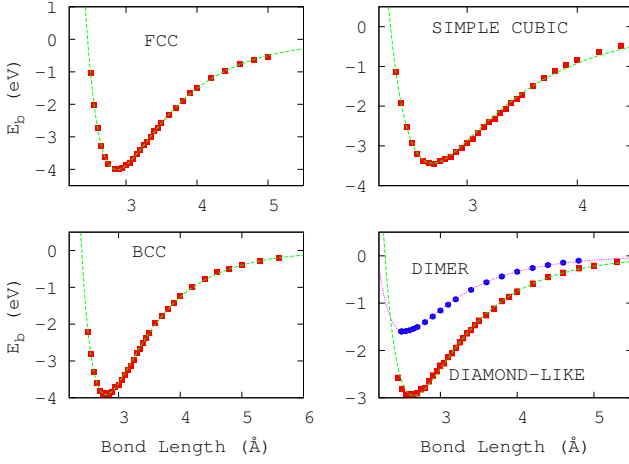


FIG. 2. Energy per Au atom as a function of distance between atoms for five phases of Au: face-centered cubic, body-centered cubic, simple cubic, the diamond-like phase and Au dimer.

The parameters λ and μ are parameterized within the E-r dependence of FCC phases (Figs. 1 and 2) as previous values for Ag⁴³ and Au⁴² did not permit a good fit of our DFT calculations.

The parameters $\alpha(n_c)$, $\beta(n_c)$ and $R_0(n_c)$ are given as functions of the coordination number of the atoms (and therefore of the phases). We suggest here the following simple functional forms:

$$\begin{aligned} \alpha(n_c) &= \alpha_\infty \left(1 + \zeta \mathcal{L} \left(\frac{n_c + n_0}{\delta} \right) \right) \\ \beta(n_c) &= \beta_\infty \left(1 + \gamma \mathcal{L} \left(\frac{n_c + \Delta}{\eta} \right) \right) \\ R_0(n_c) &= R_\infty \left[1 - \frac{\rho_0}{(1 + (n_c/\nu)^\xi)} \right], \end{aligned} \quad (6)$$

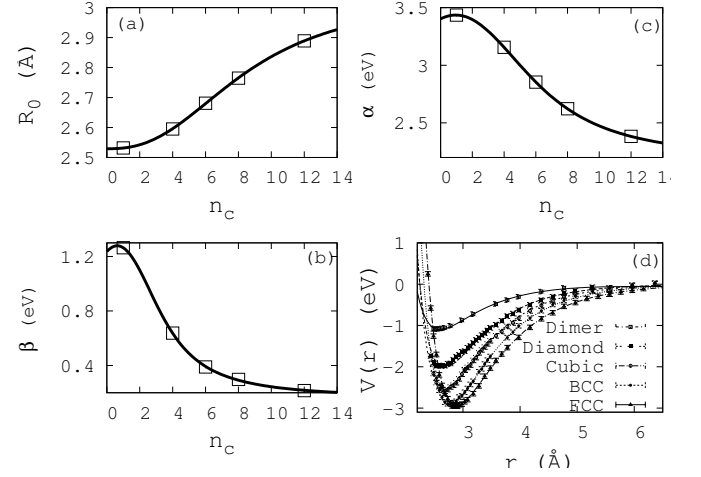


FIG. 3. DFT-parameters of the Gupta potential for the four phases of Ag: face-centered cubic, BCC, simple cubic, Ag in the diamond-like phase and Ag dimer. The fitted potentials are shown in panel (d) and the points are the corresponding DFT binding energies.

where $\mathcal{L}(x) = 2 (\exp(-x^2) - 1 + x^2) / x^4$.

A fit of the parameters to these model functional forms are performed as shown in Figs. 3 and 4 for Ag and Au, respectively. In the fitting procedure, periodic images are included such that interactions between atoms separated by distances as far as 9 Å are included. The parameters are listed in Table I.

The effect of this new parameterization of Ag and Au clusters is that in lower coordination environments (such as surfaces), the atoms become less energetic. For example, the energy per atom of an Ag dimer was found to be 1.09 eV. This compares better with the experimental value of 0.83 ± 0.02 eV⁵³ than the previously obtained values of 1.22 eV⁴³ and 1.40^{41,54}. Also the dimer bond length of 2.59 Å is in good agreement with the measured value of 2.53 Å^{53,55,56} as compared to values of 2.37 Å⁴³ and 2.43 Å^{41,54} that result from the previous parameterizations. The best DFT dimer energy so far is 0.9 eV with a corresponding dimer bond length of 2.58 Å⁵⁷. The Au dimer bond length of 2.56 Å compares very well with the experimental value of 2.47 Å⁵⁸ whereas previous parameterization sets this value at 2.3 Å⁴². The dissociation energy per atom of 1.53 eV for Au₂ is much closer to the experimental value of 1.15 eV⁵⁹ than the value of 2.42 eV that previous parameterization gives⁴². The observations made here about the properties of dimers are also valid for other low coordinations such as 2-, 3- and 4-coordinated atoms.

The implication of the weaker binding of lower coordinated atoms – as opposed to the strong binding obtained with the previous parameters^{41–43} – in studies of Ag and Au nanoclusters is that surface atoms will become more mobile. This results in the nanoclusters experiencing surface premelting at lower temperatures. The current parameterizations may, thus, be very appropriate in surface studies.

To check the validity of this parameterization for interactions beyond the cut-off distance of 3.1 Å as defined in Eq. 4, we considered the case where $n_c = 0$ and evaluated the pa-

TABLE I. Parameters of the Gupta potential for Ag and Au

	λ	μ	α_∞ (eV)	ζ	n_0	δ	β_∞ (eV)	γ	Δ	η	R_∞ (Å)	ρ_0	ν	ξ
Ag	10.167	3.105	0.1610	6.946	-0.633	1.842	2.1633	0.588	-0.952	3.414	3.039	0.168	8.482	2.517
Au	12.696	3.179	0.1471	12.1218	1.268	1.989	2.5877	0.858	2.053	3.860	2.921	0.140	6.114	3.436

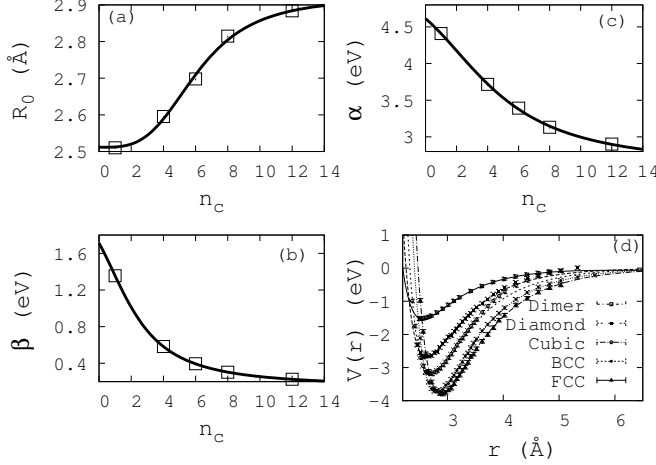


FIG. 4. DFT-parameters of the Gupta potential for the five phases of Au: face-centered cubic, BCC, simple cubic, Au in the diamond-like phase and dimer. The fitted potentials are shown in panel (d) and the points are the corresponding DFT binding energies.

rameters in Eq. 6. The corresponding potential $U_0(r)$ was extracted from Eqs. 1 - 3. For this, the central atom is interacting with one, two or three equidistant atoms that are approaching it from beyond 3.1 Å. In Fig. 5, we plot this potential for one, two and three atoms approaching the central atom. We also show the potential of the atom in the case where it participates in a dimer, in a linear chain and in a trigonal arrangement. The single atom approaches with a potential that is very similar to that of the dimer; two atoms approach with a potential very close to that of the atom in a linear chain while three atoms approach like trimers. The potential described here thus correctly describes the short-, medium- and long-range interactions in Ag and Au.

III. RELAXATION OF Ag_{55} CLUSTER AND MD DEPOSITION OF AG CLUSTERS

We performed a 2 ns MD simulation to relax a 55 atom Ag cluster at 300 K. Temperature was kept constant by using the Nosé-Hoover thermostat^{60,61} and the velocity-Verlet scheme was adopted for the MD moves. The cluster's structure was transformed from a 4-shell cluster to a 3-shell one within the first 10 ps. Figure 6 shows the density distribution as a function of distance from the central atom. The cluster is characterized by a central atom, a Ag_{12} first-shell of radius 2.74 Å, a next shell of 30 Ag atoms of radius 4.73 Å and an outermost

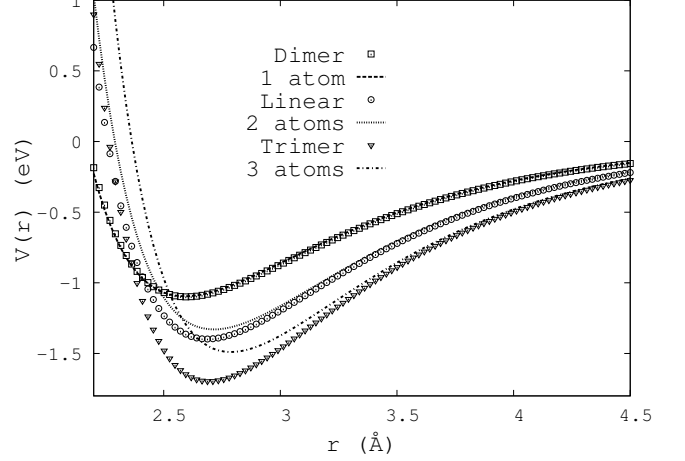


FIG. 5. The validity of the parameterization beyond $r_c=3.1$ Å. Single atom, two atoms and three atoms are clearly seen to approach the central Ag atom in such a way that the potential of the central atom closely resembles that of an atom in a dimer, a linear chain and in a trigonal arrangement of Ag atoms, respectively.

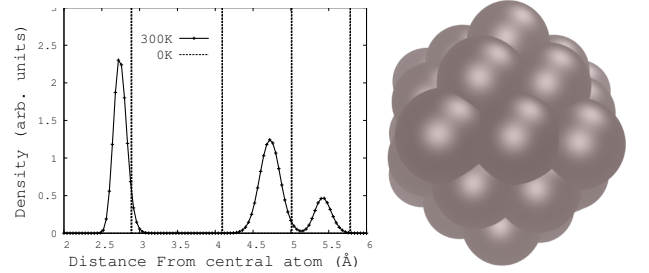


FIG. 6. Left: Density distribution as a function of distance from the central atom of a Ag_{55} cluster for the unrelaxed (thin-dotted line) and the MD-relaxed structure at 300 K (full line). The feature at 4.09 Å in the unrelaxed cluster shifts upwards and merges with the feature at 5.0 Å which shifts downwards. Right: Snapshot of MD-relaxed cluster at the end of the 2 ns simulation.

shell of 12 atoms of radius 5.45 Å. The structure of the cluster at the end of the 2 ns is shown in the right of Fig. 6.

To test further our parameters, we performed an atom by atom molecular dynamic deposition of Ag nanoclusters of up to 1000 atoms. The starting configuration was an Ag_4 cluster with four Ag atoms sitting at the corners of a square. While the cluster is undergoing relaxation at a fixed temperature, an atom is initiated far away (4 nm from the center of the formed cluster) with a kinetic energy of 2 eV and velocity pointing toward the cluster center, with the position of the atom cho-

sen randomly on the sphere of radius 4 nm. Once this atom has entered the field of the relaxing cluster (distance less than 3.5 Å from the closest cluster atom) its dynamics are included in the Nosé-Hoover thermostating scheme. The resulting cluster was relaxed for 100 ps and the process was repeated for subsequent atoms. A similar deposition process was done using the old parameters⁴³.

Figure 7 shows the evolution of the energy per atom as the cluster size grows at different temperatures using both the new and old sets of parameters. We find that the energy decreases monotonically as the cluster size increases at all temperatures except at a temperature of 500 ± 50 K, where sudden drops in energy were recorded for cluster sizes larger than 126 and 150 for the old parameters, and 150 and 192 for the new set of parameters. The cluster size of 150 is equal to the reported size beyond which a cross-over from molecular to nanometer optical behavior has been reported³². We fitted the energy per atom as a function of the cluster size with the function⁶²

$$e(T) = E(N, T)/N = e_{\infty}(T) + bN^{-1/3} + cN^{-2/3}, \quad (7)$$

where $E(N, T)$ is the total energy of an N -atom Ag cluster at temperature T (in Kelvin). The temperature dependence of the extrapolated large cluster energy, e_{∞} , is shown in the inset and reveals lower energy clusters at a temperature of 500 ± 50 K. Note the big drop in energy as the temperature is raised from 300 K to 500 K for the new parameters and the almost constant value of the energy when the old parameters are used. This indicates that the former parameters may be capable of distinguishing between the various temperature induced structural changes within Ag nanoclusters. The finding of a more stable silver cluster at a temperature of 500 ± 50 K is in accord with temperature programmed Auger, low energy electron diffraction (LEED) and thermal desorption spectroscopy study of silver deposited on Mo(111) which demonstrated that stable 3-dimensional silver clusters are formed once treated at temperatures above 300 K and below 650 K⁶³. This temperature range is also in agreement with the finding of an Ag crystallization transition between 250 and 310 °C where the agglomeration of silver atoms to form nanoclusters is favored⁶⁴.

Typical structural properties of a 561 atom Ag cluster atom-by-atom deposited at 500 K and annealed at 300 K with the new set of parameters is shown in Fig. 8. We calculated the electron diffraction pattern by using the Hartree-Fock atomic form factors as parameterized by Doyle and Turner⁶⁵. The atomic distribution with respect to the central atom of the cluster $G(r)$, shows a highly ordered nanocluster, with FCC order up to a radius of more than 1 nm. This is also confirmed by the structure factor $S(q)$, with $q = \frac{\sin \theta}{\lambda}$, λ being the wave length and θ is the Bragg's diffraction angle. All results are averages over 10 ns in time intervals of 200 fs. The assignment of the spots agree excellently with that of Khan *et al.* on Ag nanoparticles⁶⁶ and Kang *et al.* on sintered inkjet-printed Ag nanoparticles⁶⁷. In particular, the electron diffraction pattern is quite similar to the high resolution transmission electron microscopy (HRTEM) measurement of Ref. 66 on Ag nanoparticles of size 16.37 nm. $G(r)$ also shows that the 561 atoms cluster has a diameter of about 2.5 nm, which is also confirmed by size L of 24.97 ± 0.21 Å, obtained based on

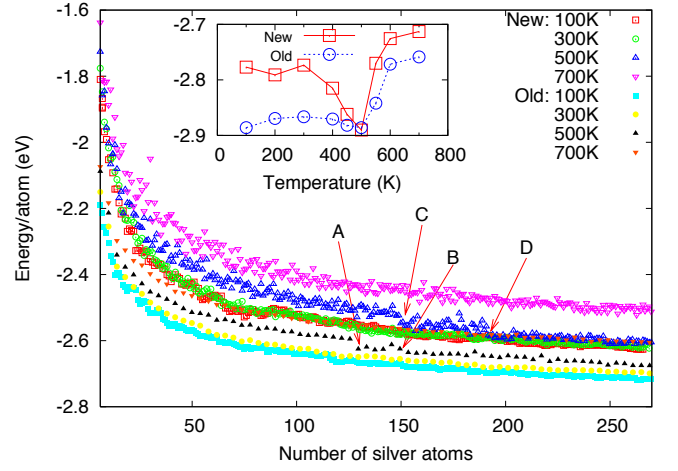


FIG. 7. The evolution of the energy per atom vs Ag cluster size at different deposition temperatures. Open symbols: new parameters, closed symbols: old⁴³. The arrows indicates points of energy drops. Inset: temperature dependence of e_{∞} (see Eqn. 7).

the position $2\theta = 38.16^\circ$ and the full-width at half-maximum (FWHM) $\sigma = 4.24^\circ$ of the (111) spot as^{66,68,69}

$$L = \frac{0.94\lambda}{\sigma \cos 2\theta}, \quad (8)$$

where σ is in radians and the wavelength $\lambda = 0.1541$ nm is used. The 2θ and σ values are obtained from a fit (in the interval $\pm 12^\circ$ around the (111) spot) with a sum of three Gaussians and a Lorentzian, with the latter centered at $q=0$. A similar calculation on a 2093 atoms cluster cut out of bulk Ag and relaxed at 300 K yielded a diameter of 4.22 ± 0.29 nm which was also quite close to its size of 4.2 nm obtained on the basis of $G(r)$.

IV. CONCLUSION

We performed DFT calculations of the binding energies of Ag and Au in five different phases: FCC, BCC, simple cubic, diamond-like and dimer. We computed the corresponding equilibrium bond lengths, binding energies and bulk moduli, and found them to compare very well with experimentally reported values. We used the binding energy versus bond length dependencies to perform a cross-phase parameterization of the widely used many-body Gupta potential for Ag and Au. The new parameters, whose coordination-number dependencies are fitted to simple analytical functions, were found to correctly describe the energetic and structural behavior of low coordinated systems. We believe that these new parameterizations should be appropriate for studies of low dimensional structures such as nanoclusters and surfaces. They may also be used to reconcile the structural differences reported for small clusters of noble metals generated using the traditional bulk-fcc-based parameters of the Gupta potential – which is susceptible to yield more strained structures – and

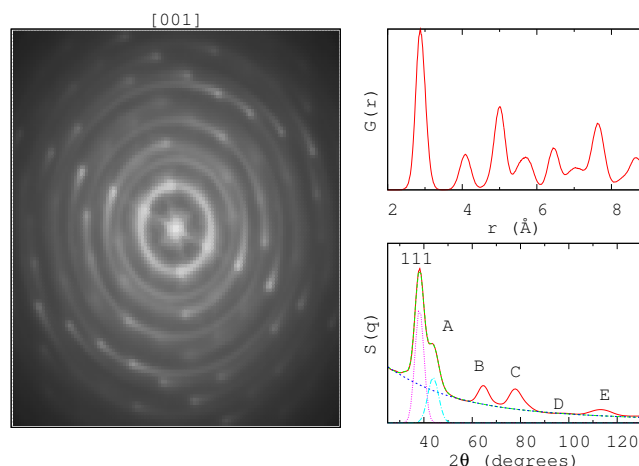


FIG. 8. The lattice structure of the 561 atom Ag nanocluster generated by MD deposition at 500 K and annealed at 300 K. The electron diffraction pattern (left) is calculated by using the Hartree-Fock parameterized form factors of Doyle and Turner⁶⁵. The (111) spot can clearly be seen. Other spots (200), (220), (311)/(222), (400) and (331)/420() are clearly visible and denoted as A, B, C, D and E, respectively. The density distribution with respect to the central atom, $G(r)$, (top-right) shows a highly ordered crystal and the structure factor $S(q)$ (lower-right) shows well defined features. The lines in the lower-right panel are for the functions used to fit the (111) spot.

the Sutton-Chen potential, which leads to less-strained structures⁴³. The current parameterization of the Gupta potential solves the problem of strain tolerance reported for the parameters of Shao *et al.*⁴³ as the broadness at the bottom of the dimer potential well is improved.

ACKNOWLEDGEMENTS

This work was supported by the Natural Sciences and Engineering Research Council of Canada (MK). Computational resources were provided by ShareNet [www.sharcnet.ca].

* jtintah@gmail.com

† mikko.karttunen@uwaterloo.ca

- ¹ J. S. Kim, E. Kuk, K. N. Yu, J.-H. Kim, S. J. Park, H. J. Lee, S. H. Kim, Y. K. Park, Y. H. Park, C.-Y. Hwang, Y.-K. Kim, Y.-S. Lee, D. H. Jeong, and M.-H. Cho, *Nanomed. Nanotechnol. Biol. Med.* **3**, 95 (2007)
- ² H. H. Lara, L. Ixtapan-Turrent, E. N. Garza Trevino, and D. K. Singh, *J. Nanobiotech.* **9** (2011)
- ³ S. Gurunathan, K.-J. Lee, K. Kalishwaralal, S. Sheikpranbabu, R. Vaidyanathan, and S. H. Eom, *Biomater.* **30**, 6341 (2009)
- ⁴ N. Portney and M. Ozkan, *Anal. Bioanal. Chem.* **384**, 620 (2006)
- ⁵ X. Huang, I. El-Sayed, W. Qian, and M. El-Sayed, *J. Am. Chem. Soc.* **128**, 2115 (2006)
- ⁶ Y.-Q. Chen and C.-J. Lu, *Sens. Actuators B Chem.* **135**, 492 (JAN 15 2009)
- ⁷ E. Filippo, A. Serra, and D. Manno, *Sens. Actuators B Chem.* **138**, 625 (2009)
- ⁸ X. He, C. Hu, H. Liu, G. Du, Y. Xi, and Y. Jiang, *Sens. Actuators B Chem.* **144**, 289 (2010)
- ⁹ M. R. H. Nezhad, J. Tashkhourian, and J. Khodaveisi, *J. Iran. Chem. Soc.* **7**, S83 (2010)
- ¹⁰ R. F. Ngece, N. West, P. M. Ndagili, R. A. Olowu, A. Williams, N. Hendricks, S. Mailu, P. Baker, and E. Iwuoha, *Int. J. Electrochem. Sci.* **6**, 1820 (2011)
- ¹¹ M. S. Bootharaju and T. Pradeep, *Langmuir* **27**, 8134 (2011)
- ¹² H. Lee, K. Chou, and K. Huang, *Nanotechnology* **16**, 2436 (2005)
- ¹³ D. Chen, X. Qiao, X. Qiu, and J. Chen, *J. Mater. Sci.* **44**, 1076 (2009)
- ¹⁴ S. L.-C. Hsu and R.-T. Wu, *Mater. Lett.* **61**, 3719 (2007)
- ¹⁵ H. Lee, K. Chou, and Z. Shih, *Int. J. Adhes. Adhes.* **25**, 437 (2005)

- ¹⁶ A. Hu, J. Y. Guo, H. Alarifi, G. Patane, Y. Zhou, G. Compagnini, and C. X. Xu, *Appl. Phys. Lett.* **97** (2010)
- ¹⁷ Y.-C. Hung, W.-T. Hsu, T.-Y. Lin, and L. Fruk, *Appl. Phys. Lett.* **99** (2011)
- ¹⁸ A. Ashkin, *Phys. Rev. Lett.* **24**, 156 (1970)
- ¹⁹ A. Ashkin, J. M. Dziedzic, J. E. Bjorkholm, and S. Chu, *Optics. Lett.* **11**, 288 (1986)
- ²⁰ M. Liu, T. Zentgraf, Y. Liu, G. Bartal, and X. Zhang, *Nature Nanotechnol.* **5**, 570 (2010)
- ²¹ F. Svedberg and M. Kall, *Faraday Disc.* **132**, 35 (2006)
- ²² S. R. Bhattacharyya, D. Datta, I. Shyjumon, B. M. Smirnov, T. K. Chini, D. Ghose, and R. Hippler, *J. Phys. D Appl. Phys.* **42** (2009)
- ²³ C.-A. J. Lin, C.-H. Lee, J.-T. Hsieh, H.-H. Wang, J. K. Li, J.-L. Shen, W.-H. Chan, H.-I. Yeh, and W. H. Chang, *J. Med. Biol. Eng.* **29**, 276 (2009)
- ²⁴ M. A. MacDonald, D. M. Chevrier, P. Zhang, H. Qian, and R. Jin, *J. Phys. Chem. C* **115**, 15282 (2011)
- ²⁵ H. Qian, M. Zhu, U. N. Andersen, and R. Jin, *J. Phys. Chem. A* **113**, 4281 (2009)
- ²⁶ H. Wei, Z. Wang, L. Yang, S. Tian, C. Hou, and Y. Lu, *Analyst* **135**, 1406 (2010)
- ²⁷ J. T. Petty, C. Fan, S. P. Story, B. Sengupta, A. S. J. Iyer, Z. Prudowsky, and R. M. Dickson, *J. Phys. Chem. Lett.* **1**, 2524 (2010)
- ²⁸ M. Takesue, T. Tomura, M. Yamada, K. Hata, S. Kuwamoto, and T. Yonezawa, *J. Am. Chem. Soc.* **133**, 14164 (2011)
- ²⁹ D. Reinhard, B. Hall, D. Ugarte, and R. Monot, *Phys. Rev. B* **55**, 7868 (1997)
- ³⁰ M. Blom, D. Schooss, J. Stairs, and M. Kappes, *J. Chem. Phys.* **124** (2006)
- ³¹ X. Yang, W. Cai, and X. Shao, *J. Phys. Chem. A* **111**, 5048 (2007)
- ³² H.-C. Weissker and C. Mottet, *Phys. Rev. B* **84** (2011)

- ³³ L. Jensen, L. L. Zhao, and G. C. Schatz, *J. Phys. Chem. C* **111**, 4756 (2007)
- ³⁴ F. Cleri and V. Rosato, *Phys. Rev. B* **48**, 22 (1993)
- ³⁵ K. Michaelian, N. Rendon, and I. Garzon, *Phys. Rev. B* **60**, 2000 (1999)
- ³⁶ A. P. Sutton and J. Chen, *Phil. Mag. Lett.* **61** (1990)
- ³⁷ J. Doye and D. Wales, *New J. Chem.* **22**, 733 (1998)
- ³⁸ J. Mei, J. W. Davenport, and G. W. Fernando, *Phys. Rev. B* **43**, 4653 (1991)
- ³⁹ T. Shibata, B. A. Bunker, Z. Y. Zhang, D. Meisel, C. F. Vardeman, and J. D. Gezelter, *J. Am. Chem. Soc.* **124**, 11989 (2002)
- ⁴⁰ S. Zhao, S. Wang, and H. Ye, *J. Phys. Soc. Jpn.* **70**, 2953 (2001)
- ⁴¹ X. Wu, Y. Wu, X. Kai, G. Wu, and Y. Chen, *Chem. Phys.* **390** (2011)
- ⁴² F. Pittaway, L. O. Paz-Borbon, R. L. Johnston, H. Arslan, R. Ferrando, C. Mottet, G. Barcaro, and A. Fortunelli, *J. Phys. Chem. C* **113**, 9141 (2009)
- ⁴³ X. Shao, X. Liu, and W. Cai, *J. Chem. Theory Comput.* **1**, 762 (2005)
- ⁴⁴ P. Blaha, K. Schwarz, P. Sorantin, and S. B. Trickey, *Comput. Phys. Commun.* **59**, 399 (1990)
- ⁴⁵ J. P. Perdew, K. Burke, and M. Ernzerhof, *Phys. Rev. Lett.* **77**, 3865 (1996)
- ⁴⁶ C. Kittel, *Introduction to Solid State Physics*, 4th ed. (John Wiley & Sons, Inc., 1971)
- ⁴⁷ J. Neighbours and G. Alers, *Phys. Rev.* **111**, 707 (1958)
- ⁴⁸ R. L. Chantry, W. Siriwatcharapiboon, S. L. Horswell, A. J. Logsdail, R. L. Johnston, and Z. Y. Li, *J. Phys. Chem. C* **116**, 10312 (2012)
- ⁴⁹ M. Needels, R. A. M., P. D. Bristowe, and J. D. Joannopoulos, *Phys. Rev. B* **46**, 9768 (1992)
- ⁵⁰ P. Soderlind, *Phys. Rev. B* **66**, 176201 (2002)
- ⁵¹ Q. M. Wei, X. Y. Liu, and A. Misra, *Appl. Phys. Lett.* **98** (2011)
- ⁵² F. Cleri and V. Rosato, *Phys. Rev. B* **48**, 22 (1993)
- ⁵³ M. Morse, *Chem. Rev.* **86**, 1049 (1986)
- ⁵⁴ F. R. Negreiros, Z. Kuntova, G. Barcaro, G. Rossi, R. Ferrando, and A. Fortunelli, *J. Chem. Phys.* **132** (2010)
- ⁵⁵ V. Beutel, H. G. Kramer, G. L. Bhale, M. Kuhn, K. Weyers, and W. Demtroder, *J. Chem. Phys.* **98**, 2699 (1993)
- ⁵⁶ G. Wang, J. BelBruno, S. Kenny, and R. Smith, *Phys. Rev. B* **69** (2004)
- ⁵⁷ S. Nigam and C. Majumder, *Langmuir* **26**, 18776 (2010)
- ⁵⁸ K. Huber and H. Hertzberg, *Molecular Spectra and Molecular Structure Constants of Diatomic Molecules*, Vol. IV (van Nostrand, New York, 1979)
- ⁵⁹ A. James, P. Kowalczyk, B. Simard, J. Pinegar, and M. Morse, *J. Mol. Spectrosc.* **168**, 248 (1994)
- ⁶⁰ S. Nosé, *Mol. Phys.* **52**, 255 (1984), ISSN 0026-8976
- ⁶¹ W. G. Hoover, *Phys. Rev. A* **31**, 1695 (1985)
- ⁶² W. Huang, X. Lai, and R. Xu, *Chem. Phys. Lett.* **507**, 199 (2011)
- ⁶³ K. Song, W. Chen, V. Yeh, Y. Liao, P. Tsao, and M. Lin, *Surface Science* **478**, 145 (2001)
- ⁶⁴ R. J. T. Houk, B. W. Jacobs, F. El Gabaly, N. N. Chang, A. A. Talin, D. D. Graham, S. D. House, I. M. Robertson, and M. D. Allendorf, *Nano Lett.* **9**, 3413 (2009)
- ⁶⁵ P. A. Doyle and P. S. Turner, *Acta. Cryst. A* **A 24**, 390 (1968)
- ⁶⁶ M. A. M. Khan, S. Kumar, M. Ahamed, S. A. Alrokayan, and M. S. AlSalhi, *Nano. Res. Lett.* **6** (2011)
- ⁶⁷ J. S. Kang, J. Ryu, H. S. Kim, and H. T. Hahn, *J. Electron. Mater.* **40**, 2268 (2011)
- ⁶⁸ H. P. Klug and L. E. Alexander, *X-ray diffraction procedures for polycrystalline and amorphous material* (Wiley, New York, 1954)
- ⁶⁹ R. Govindaraj, R. Kesavamoorthy, R. Mythili, and B. Viswanathan, *J. Appl. Phys.* **90**, 958 (2001)